Quasiclassical State-Selected Trajectory Study of O + H_3^+ Reaction

Richard E. Cook and Charles W. Eaker*

University of Dallas, 1845 E. Northgate Drive, Irving, Texas 75062

Received: May 26, 2004; In Final Form: August 27, 2004

We report the results of a quasiclassical trajectory study of the reaction of O + H_3^+. In this study, action-angle fast Fourier transform methods are used (a) to prepare the H_3^+ reactants in specific vibrational states and (b) to analyze the vibrational states of the H_2O^+ products. There are two possible product channels for this reaction: (1) O + $H_3^+ \rightarrow OH^+ + H_2$ ($\Delta E_1 = -57$ kJ/mol) and (2) O + $H_3^+ \rightarrow H_2O^+ + H$ ($\Delta E_2 = -158$ kJ/mol). Channel 1 is the predominant reaction channel even though channel 2 is 101 kJ/mol lower in energy. Channel 2 corresponds to the very unusual donation of a H_2^+ ion to a neutral species. Our results show the effects of H_3^+ vibrational state and O + H_3^+ collisional energy on the dynamics of the reaction. A detailed analysis of the product states and reaction mechanism for each product channel is presented.

Introduction

There are two possible product channels for this reaction of O + H_3^+:

$$O + H_3^+ \rightarrow OH^+ + H_2 \qquad \Delta E_1 = -57 \text{ kJ/mol} \quad (1)$$

$$O + H_3^+ \rightarrow H_2O^+ + H \qquad \Delta E_2 = -158 \text{ kJ/mol} \quad (2)$$

Channel 1 is the predominant reaction channel even though channel 2 is 101 kJ/mol lower in energy. The reaction O + $H_3^+ \rightarrow H_2O^+ + H$ is the only known example of H_2^+ donation from H_3^+ to a neutral species. Other H_3^+ ion−molecule reactions show only H^+ transfer. The reaction of O with H_3^+ has been identified as playing an important role in the synthesis of H_2O in interstellar molecular clouds.

Fehsenfeld[1] reported in 1976 the results of an experimental study of this reaction. His results were obtained in room-temperature flowing afterglow experiments at the NOAA Aeronomy Research Laboratory in Boulder, Colorado. Fehsenfeld measured the rate constant for the O + H_3^+ reaction, $8 \pm 4 \times 10^{-10}$ cm^3 s^{-1}, but was unable to determine the relative importance of the two reaction channels. This was because both products were rapidly converted to H_3O^+ in a reaction with H_2, the source gas in his experiment for the production of H_3^+.

More recently, a theoretical study of the reaction of O + H_3^+ was reported by Bettens et al.[2] in 1999. In this work, they constructed a complete multidimensional potential energy surface (PES) for this system. The PES is given by an interpolation of Taylor expansions centered on 727 data points. The potential energy at each of the data points was determined using GAUSSIAN94[3] at the MP2/6-311+G(2d,p) level. The geometries of the data points were selected from a search for local minima and saddle points on the surface and from running O + H_3^+ and $OH^+ + H_2$ trajectories. The accuracy of the fitted PES was 0.35 kJ/mol on the basis of a test of 1000 random configurations spanning an energy range of 220 kJ/mol. The exoergicity of the PES for channel 1 is −56 kJ/mol and −166 kJ/mol for channel 2. This is in good agreement with the experimental values of −57 and −158 kJ/mol.

After constructing the PES, Bettens et al. evaluated 2000 trajectories for each of seven different initial relative translational energies O + H_3^+ ranging from 4.6 to 17.9 kJ/mol. On the basis of the cross sections calculated from these trajectories, they were able to determine the value of the thermal rate constant between 0 and 500 K. Their result for the combined (channels 1 and 2) O + H_3^+ rate constant at 300 K was 9.392×10^{-10} cm^3 s^{-1}. This compares favorably with the Fehsenfeld experimental result of $8 \pm 4 \times 10^{-10}$ cm^3 s^{-1}. Their trajectory study further showed that the unusual formation of H_2O^+ in the O + H_3^+ reaction occurs in a two-step process: (1) O extracts H^+ from H_3^+ to form OH^+ and H_2, which is followed by (2) H extraction from H_2 by OH^+ to form H_2O^+.

The purpose of this paper is to extend the work of Bettens et al. (a) to determine the effect of the initial H_3^+ vibrational state in the collision of O with H_3^+, (b) to provide a more complete analysis of the product states in both channels, and (c) to study in more detail the reaction pathways, particularly in the H_2O^+ + H product channel.

Description of Calculations

We used the Bettens et al. OH_3^+ PES and a modified version of their classical trajectory program. The trajectory program was modified to generate the H_3^+ initial coordinates and momentum using a fast Fourier transform (FFT) method[4] that we have described previously. The first step in this method is to do an exact FFT semiclassical quantization[5] of the H_3^+ ion for each of the vibrational states of interest. We did the FFT quantization of the first three H_3^+ vibrational states: (000), (010)+(001), and (100). The notation ($n_1n_2n_3$) corresponds to (symmetric stretch, bend, asymmetric stretch) quanta. The second state, (010)+(001), is a degenerate state involving the bend and asymmetric stretch modes. As shown in Table 1, the vibrational energies of these states are 52.3, 81.9, and 90.9 kJ/mol. To efficiently determine these vibrational states, we used a fifth-degree Simons−Parr−Finlan[6] expansion to fit the H_3^+ region of the OH_3^+ PES. In the Bettens et al. O + H_3^+ trajectory study, the H_3^+ was given an initial vibrational energy of 47.3 kJ/mol using a microcanonical sampling technique.

For each trajectory, the O and H_3^+ centers of mass were separated by 20 bohr, the reactants were randomly oriented,

* Corresponding author. E-mail address: eaker@udallas.edu.

10.1021/jp047712m CCC: $27.50
Published on Web 10/15/2004

TABLE 1: Initial O + H_3^+ Collisional Energies and H_3^+ Vibrational States

label	collisional energy (kJ/mol)	H_3^+ vibrational states[a]	vibrational energy (kJ/mol)
4_{000}	4.59	(000)	52.3
13_{000}	13.1	(000)	52.3
$4_{01/21/2}$	4.59	(010)+(001)	81.9
$13_{01/21/2}$	13.1	(010)+(001)	81.9
4_{100}	4.59	(100)	90.9
13_{100}	13.1	(100)	90.9

[a] $(n_1n_2n_3)$ = (symmetric stretch, bend, asymmetric stretch).

TABLE 2: Reaction Cross Sections

label	products	cross section (Å^2)
4_{000}	$OH^+ + H_2$	89.9 ± 2.5
	$H_2O^+ + H$	7.1 ± 1.0
13_{000}	$OH^+ + H_2$	52.3 ± 2.4
	$H_2O^+ + H$	1.6 ± 0.5
$4_{01/21/2}$	$OH^+ + H_2$	93.8 ± 2.5
	$H_2O^+ + H$	9.3 ± 1.2
$13_{01/21/2}$	$OH^+ + H_2$	54.5 ± 2.4
	$H_2O^+ + H$	3.2 ± 0.7
4_{100}	$OH^+ + H_2$	89.0 ± 2.5
	$H_2O^+ + H$	9.2 ± 1.2
13_{100}	$OH^+ + H_2$	51.8 ± 2.4
	$H_2O^+ + H$	2.7 ± 0.7

and the H_3^+ was given zero rotational angular momentum. The impact parameter *b* was sampled from a distribution of values between 0 and 15 bohr. The distribution was prepared so that the probability of a trajectory having an impact parameter between *b* and *b* + d*b* was proportional to *b*. For each of the three sets of vibrational energies, two different initial relative collisional energies were used: 0.00175 hartree (4.59 kJ/mol) and 0.0050 hartree (13.1 kJ/mol). The six sets of initial conditions are shown in Table 1. Notice that in Table 1 and the later tables we have used the notation 4_{n1n2n3} and 13_{n1n2n3} to identify different sets of initial conditions (4 for 4.59 kJ/mol and 13 for 13.1 kJ/mol collisional energies and $n_1n_2n_3$ for the vibrational states). For each set of initial conditions, we ran 1000 trajectories.

Results

Reported in Table 2 are the cross sections in Å^2 for each of the two product channels. The initial conditions used by Bettens et al. are similar to our 4_{000} and 13_{000} cases and their calculated cross sections are consistent with our calculations. For example, at 4.59 kJ/mol we calculate 89.9 ± 2.9 Å^2 for $OH^+ + H_2$ and 7.1 ± 1.0 Å^2 for $H_2O^+ + H$ and the Bettens paper reports cross sections of 90.9 ± 1.5 and 7.9 ± 0.5 Å^2. At 13.1 kJ/mol we calculate 52.3 ± 2.4 and 1.6 ± 0.5 Å^2 and their paper reports 54.7 ± 1.2 and 2.8 ± 0.5 Å^2. Both of these calculations show that the reaction cross sections decrease as the initial translational energy increases and the percentage of $H_2O^+ + H$ products decrease as translational energy increases. We calculate that the percentage of $H_2O^+ + H$ products is 7.3% for 4.59 kJ/mol collisions and 3.0% at 13.1 kJ/mol collisions.

Increasing the H_3^+ vibrational energy produces a small increase in $H_2O^+ + H$ cross sections. At 4.59 kJ/mol the cross sections increases from 7.1 Å^2 for 4_{000} to 9.3 Å^2 for $4_{01/21/2}$ and 9.2 Å^2 for 4_{100}. For the higher energy collisions, there is even a larger relative increase from 1.6 Å^2 for 13_{000} to 3.2 and 2.7 Å^2 for $13_{01/21/2}$ and 13_{100}. Increasing the H_3^+ vibrational energy has essentially no effect on the $OH^+ + H_2$ cross sections.

The final values of the coordinates and momentum for each of the trajectories were analyzed to determine how energy was distributed among the products. The results for the $OH^+ + H_2$ channel are shown in Table 3. It is interesting that each diatomic product receives about 50% of the available energy. The internal energy and translational energy are about equally shared for H_2 but for OH^+ the energy is almost all internal energy. The disposal of energy in the $H_2O^+ + H$ product channel is shown in Table 4. We find that more than 80% of the available energy is dumped into the H_2O^+ ion. As was the case for OH^+, less than 2% of the H_2O^+ product energy is in translational energy.

TABLE 3: Disposal of Energy into $OH^+ + H_2$ Products

label	total energy available (kJ/mol)	OH^+ translational energy	OH^+ internal energy	H_2 translational energy	H_2 internal energy
4_{000}	112	2.1%	52.8%	18.1%	27.0%
13_{000}	121	2.8%	50.4%	23.9%	22.9%
$4_{01/21/2}$	142	2.0%	55.4%	17.0%	25.6%
$13_{01/21/2}$	151	2.6%	52.3%	22.3%	22.7%
4_{100}	151	1.8%	45.4%	15.5%	37.6%
13_{100}	159	2.3%	42.2%	19.6%	35.9%

TABLE 4: Disposal of Energy into $H_2O^+ + H$ Products

label	total energy available (kJ/mol)	H translational energy	H_2O^+ translational energy	H_2O^+ internal energy
4_{000}	222	20.0%	1.1%	78.9%
13_{000}	230	14.9%	0.8%	84.2%
$4_{01/21/2}$	252	13.7%	0.8%	85.6%
$13_{01/21/2}$	261	12.8%	0.7%	86.5%
4_{100}	261	15.8%	0.9%	83.3%
13_{100}	269	18.4%	1.0%	80.6%

TABLE 5: Weighted Average Values and (Ranges) of H_2O^+ Quantum Numbers

label	J	$v_{sym\ str}$	v_{bend}	$v_{asym\ str}$
4_{000}	13.3 (1.4−30.5)	0.9 (0−2.5)	3.0 (1.0−8.0)	0.4 (0−2.3)
13_{000}	11.2 (3.4−24.2)	1.4 (0.1−2.7)	4.3 (1.9−7.5)	0.1 (0−2.2)
$4_{01/21/2}$	16.1 (9.8−31.8)	1.3 (0.1−2.7)	3.4 (1.2−5.8)	0.8 (0−2.0)
$13_{01/21/2}$	18.1 (7.6−31.5)	1.0 (0−1.2)	4.1 (1.7−6.2)	0.9 (0−3.3)
4_{100}	17.2 (5.7−35.3)	1.0 (0−3.3)	3.6 (0−6.9)	0.8 (0−3.1)
13_{100}	18.7 (4.6−32.8)	1.0 (0.3−2.3)	3.1 (0.2−8.7)	0.9 (0−3.5)

For the $H_2O^+ + H$ products, we used the approximate FFT method[5] to determine the vibrational and rotational quantum states of H_2O^+ products. These results are shown in Table 5. The results are reasonably consistent for the different sets of initial conditions. The H_2O^+ product is rotationally and vibrationally excited. The excited bend mode is the most excited vibrational mode with an average value of v_{bend} of 3.6. The symmetric stretch has about one quanta of energy. However, we do find some differences due to the initial conditions. For example, O collisions with vibrationally excited H_3^+ give higher average values of the total rotational quantum number *J* and more energy in the H_2O^+ asymmetric stretch. Vibrationally excited H_3^+ produces H_2O^+ with an average *J* around 16 and a range from 5 to 35; the corresponding results for H_2O^+ from ground-state H_3^+ are an average *J* of 12 and a range of 1−30. The symmetric and asymmetric stretch modes of H_2O^+ have about one quanta of excitation when the H_3^+ is vibrationally excited; there is very little asymmetric stretch excitation in H_2O^+ from the reaction of O and H_3^+ in the ground vibrational state.

Table 6 gives the partition of vibrational and rotational energies for the $OH^+ + H_2$ products. For both OH^+ and H_2, the amount of energy in vibration is two to three times greater than the energy in rotation. For the trajectories in which the H_3^+ was in the 100 excited vibrational state, 4_{100} and 13_{100}, there is almost twice as much vibrational energy in the H_2 products (as shown in the last column of Table 6).

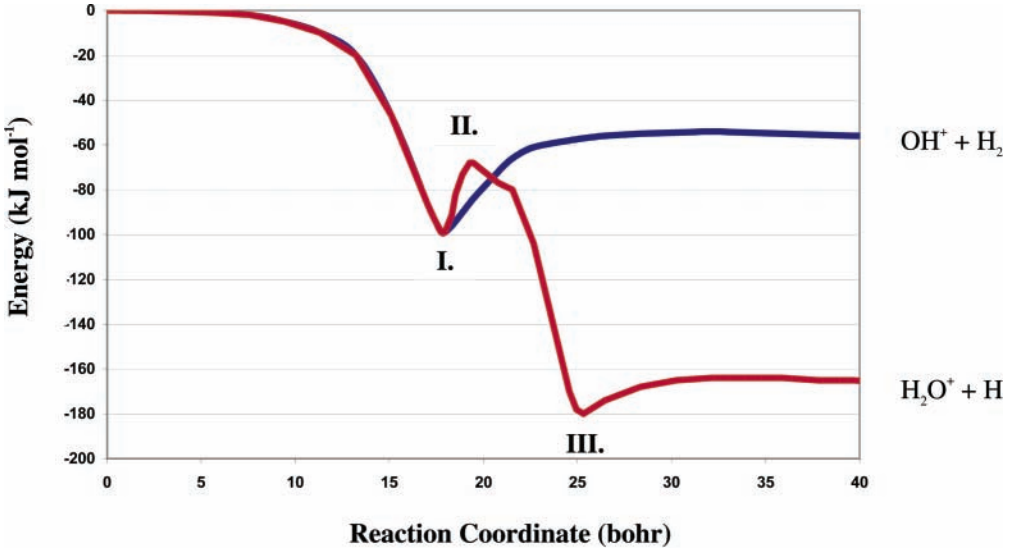

Figure 1. The minimum energy path along the path of steepest descents. The geometries of the critical points (I, II, and III) are shown in Figure 2.

TABLE 6: OH^+ and H_2 Weighted Average Rotational and Vibrational Energies and (Ranges)

label	total energy available (kJ/mol)	OH^+		H_2	
		E_{rot} (kJ/mol)	E_{vib} (kJ/mol)	E_{rot} (kJ/mol)	E_{vib} (kJ/mol)
4_{000}	112	18.0 (0−86)	41.3 (0−108)	8.6 (0−59)	21.7 (0−101)
13_{000}	121	12.3 (0−74)	46.0 (0−112)	6.8 (0−53)	19.4 (0−65)
$4_{01/21/2}$	142	22.9 (0−126)	53.6 (0−123)	12.2 (0−77)	24.2 (0−117)
$13_{01/21/2}$	151	21.1 (0−124)	56.3 (2−126)	11.1 (0−76)	23.6 (0−108)
4_{100}	151	19.0 (0−116)	49.5 (0−138)	11.2 (0−105)	45.6 (0−118)
13_{100}	159	19.2 (0−148)	48.0 (0−135)	9.7 (0−81)	47.6 (0−135)

Reaction Mechanisms

The minimum energy paths for the two product channels are shown in Figure 1. Figure 2 shows the molecular geometries at the critical points along the minimum energy paths. Figure 3 is a contour plot of the potential energy surface. The contour plot was constructed by specifying R_{O-Ha} and R_{O-Hb} and then optimizing the other four radii to give the lowest potential energy at each point. Conveniently displayed on this plot are both product channels and the local C_{2v} minimum (critical point I in Figures 1 and 2) at $R_{O-Ha} = 4.603$ bohr and $R_{O-Hb} = 2.081$ bohr. Notice the differences in the topology of the two product channels: the broad exit channel for the $OH^+ + H_2$ products and the much narrower exit channel for the $H_2O^+ + H$ products. Another more subtle difference is the dissimilarity between the smooth change in geometric configuration in going from $O + H_3^+$ to $OH^+ + H_2$ and the abrupt change in configuration across the ridge that separates the C_{2v} minimum from the $H_2O^+ + H$ products. The minimum in this ridge occurs at an energy of about −77.5 kJ/mol with $R_{O-Ha} = 4.0135$ bohr and $R_{O-Hb} = 1.9300$ bohr. The abrupt change in configuration can be seen by comparing the radii (R_{O-Ha}, R_{O-Hb}, R_{O-Hc}, R_{Ha-Hb}, R_{Ha-Hc}, R_{Hb-Hc}) at two points ±0.0005 bohr from the minimum geometry on the ridge. The radii on the C_{2v} side are (4.0140, 1.9300, 4.5473, 2.2621, 1.4243, 2.6174) compared to the radii (4.0130, 1.9300, 4.0133, 4.4312, 1.4398, 4.4869) found on the $H_2O^+ + H$ side of the ridge. Notice the change in the $O-H_c$ distance from 4.5473 to 4.0133 bohr and the big changes in the H_a-H_b and H_b-H_c distances.

In light of these observations of the characteristics of the potential energy surface, we will now turn to the trajectory results. One of the surprises that we found was that the reaction times for the $OH^+ + H_2$ and $H_2O^+ + H$ product channels were essentially the same. For the 4.59 kJ/mol collisions, the $OH^+ + H_2$ and $H_2O^+ + H$ products were formed in about 0.8 ps (0.6 ps for the 13.1 kJ/mol trajectories). The detailed values are shown in Table 7. These results were surprising because we had expected that the $OH^+ + H_2$ products would be formed faster with a one-step process and that forming H_2O^+ would take longer as it is formed in two steps. One reason for this is that the average impact parameter (also shown in Table 7) for the $OH^+ + H_2$ channel is 2−3 bohr larger than that of the H_2O^+

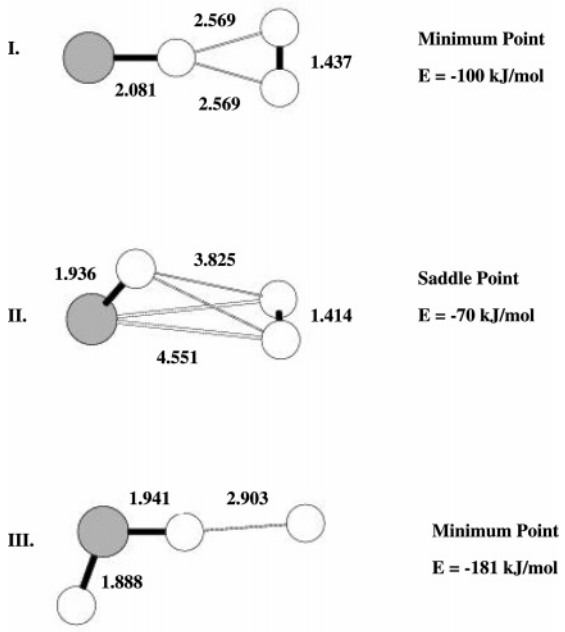

Figure 2. Critical points (minima and saddle point) along reaction coordinate to $H_2O^+ + H$. The bond distances are in bohrs.

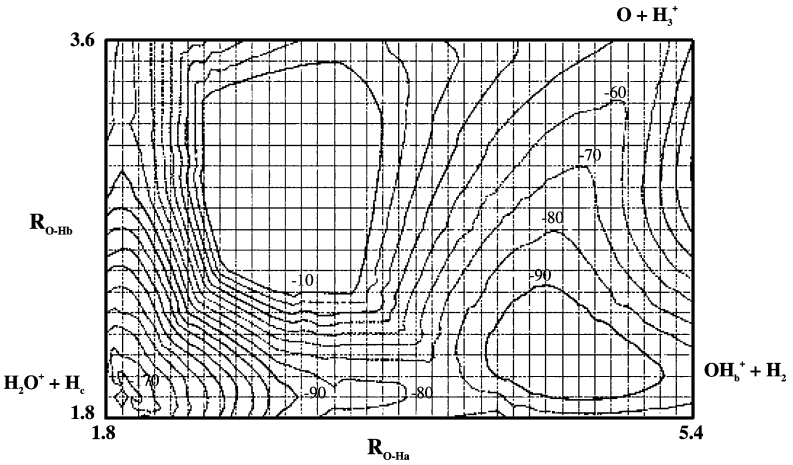

Figure 3. Contour plot of R_{O-Hb} vs R_{O-Ha}. The four other radii have been optimized to produce the lowest energy at each point. The bond distances are in bohrs and the energies are in kJ/mol. Each contour line represents 10 kJ/mol.

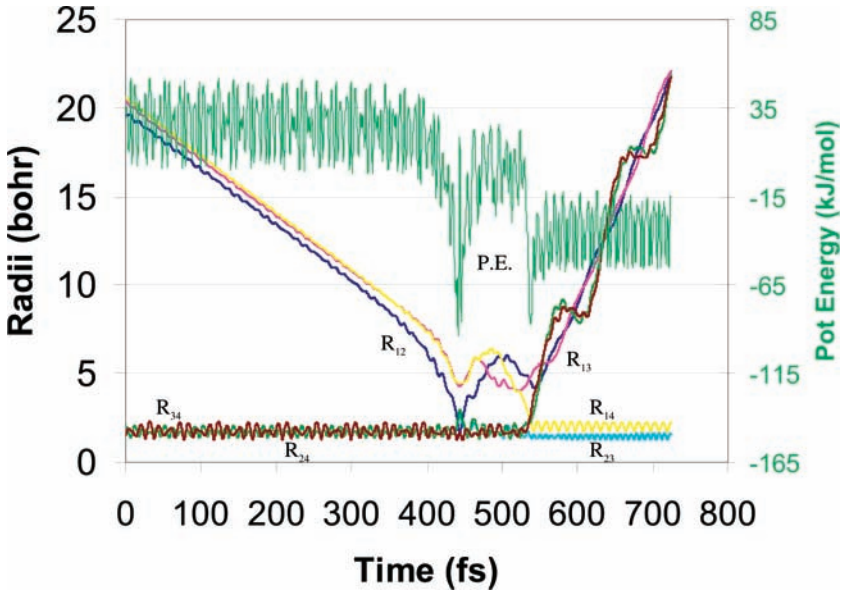

Figure 4. Radii and potential energy graph for a $OH^+ + H_2$ trajectory (a 4_{000} trajectory with $b = 8.4$ bohr).

TABLE 7: Weighted Average Reaction Times and Impact Parameters and (Ranges)

	$OH^+ + H_2$		$H_2O^+ + H$	
label	reaction time (ps)	*b* (bohr)	reaction time (ps)	*b* (bohr)
4_{000}	0.86 (0.45−1.97)	8.3 (0.5−13.4)	0.85 (0.58−1.72)	4.8 (0.8−10.4)
13_{000}	0.57 (0.38−1.32)	6.3 (0.5−10.4)	0.57 (0.45−0.85)	3.9 (1.4−7.2)
$4_{01/21/2}$	0.76 (0.48−1.82)	8.3 (0.4−13.0)	0.75 (0.53−1.45)	6.1 (1.5−11.0)
$13_{01/21/2}$	0.54 (0.33−1.32)	6.5 (0.4−10.3)	0.60 (0.38−1.32)	4.2 (1.9−7.8)
4_{100}	0.81 (0.45−1.90)	8.3 (0.3−13.5)	0.80 (0.53−1.47)	6.0 (0.9−11.9)
13_{100}	0.56 (0.33−1.45)	6.2 (0.3−10.8)	0.62 (0.38−1.20)	3.8 (0.5−6.8)

+ H channel. With a larger average impact, it takes longer for the O + H_3^+ reactants to reach the reaction zone.

To get a more detailed picture of the reaction mechanisms for each of the product channels, we constructed radii and potential energy graphs of individual trajectories. Two examples of these graphs are shown in Figures 4 and 5.

$OH^+ + H_2$ Mechanism. Figure 4 is the graph of a 4_{000} trajectory with $b = 8.4$ bohr that produces $OH^+ + H_2$. This trajectory is typical of the $OH^+ + H$ trajectories with a reaction time and impact parameter consistent with the averages for these products. During the first 400 fs, the O atom is approaching the H_3^+ ion. The average potential energy remains fairly constant around 30 kJ/mol (the oscillations are due to the H_3^+ vibration). When the O−H distances reach about 5 bohr, the potential energy decreases rapidly as the atoms approach the configuration of the local minimum at −100 kJ/mol (point I in Figures 1 and 2). At this point, atom H_a is closest to the O atom (R_{12}). However, then the O atom moves away from the H_3^+ ion. Following a rotation of the H_3^+ ion, H_c becomes closest to the O atom (R_{14}). This time the O captures the H_c proton and the H_a-H_c (R_{24}) and H_b-H_c (R_{34}) bonds are broken. The final products are OH_c^+ (R_{14}) and H_aH_b (R_{23}). Many of the trajectories studied showed that the proton that is ultimately transferred to the O atom is not the first hydrogen atom of closest approach. Sometimes this happens, but typically there are two or more collisions of the O atom with the H_3^+ ion before the exchange occurs that leads to separation and the final products.

$H_2O^+ + H$ Mechanism. Figure 5 is a 4_{000} trajectory with $b = 5.5$ bohr that produces $H_2O^+ + H$. This trajectory is typical of trajectories that produce H_2O^+. It has several similarities to

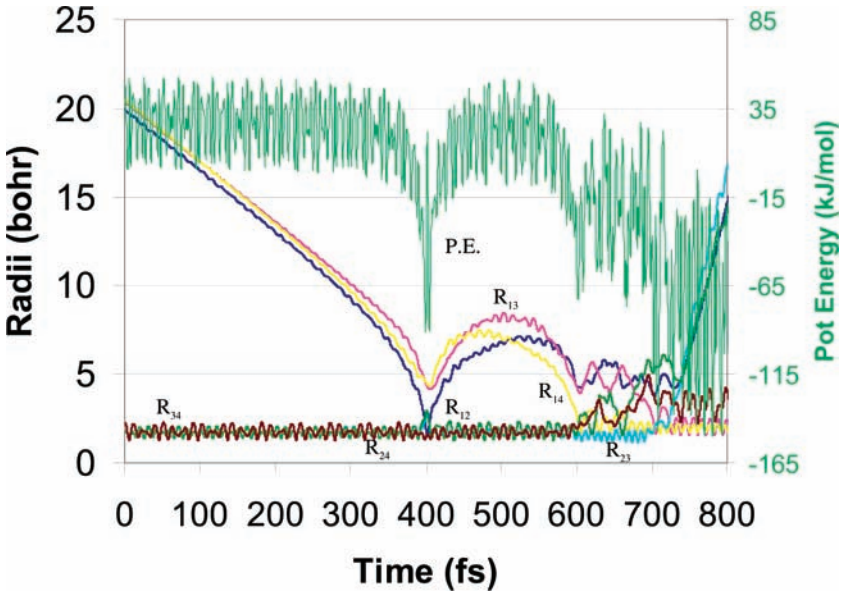

Figure 5. Radii and potential energy graph for a $H_2O^+ + H$ trajectory (a 4_{000} trajectory with $b = 5.5$ bohr).

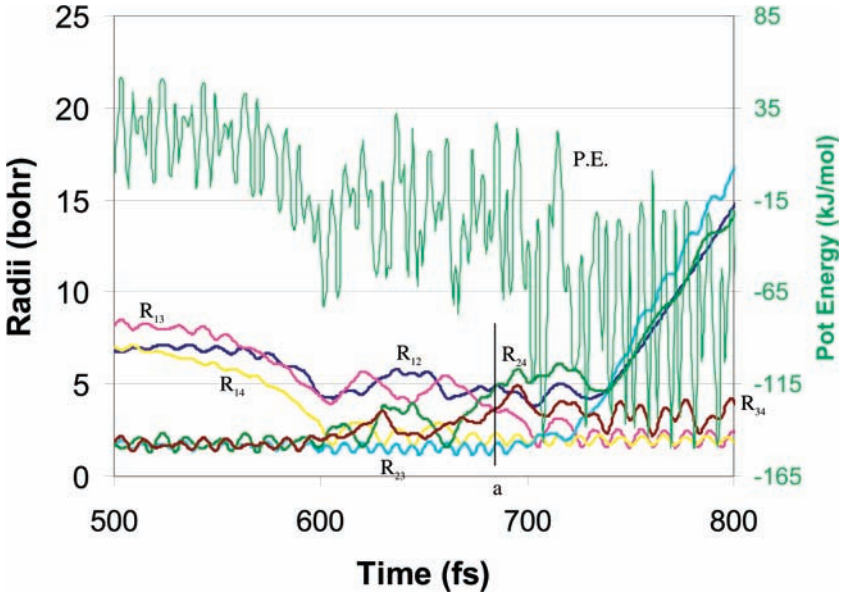

Figure 6. Radii and potential energy graph for a $H_2O^+ + H$ trajectory (a 4_{000} trajectory with $b = 5.5$ bohr) at the point of formation of H_2O^+.

the $OH^+ + H_2$ trajectory described previously. The O atom approaches the H_3^+ ion in the first 400 fs, with a sharp decrease in potential energy when the O−H distances approach 5 bohr. The O atom then bounces off H_3^+ and H_3^+ rotates. Step 1 in the H_2O^+ formation occurs at 600 fs where the proton H_c is bonded to the O atom (see R_{14}). This is shown more clearly in Figure 6 in which the time axis has been rescaled to 600−800 fs. Step 2 is the extraction of the second H, H_b in this case (see R_{13}), and this occurs around 700 fs for this trajectory. H_a rapidly separates from $H_bH_cO^+$ beginning at about 730 fs. In analyzing the $H_2O^+ + H$ trajectories, we found that in most cases the atoms assumed a "critical configuration" just prior to the step 2 hydrogen atom transfer. Figure 6 is an expanded look at the region in Figure 5 where H_2O^+ gets formed. The vertical line labeled "a" in Figure 6 indicates this configuration for which R_{12} (O−H_a) ≈ R_{24} (H_a−H_c) ≈ 5 bohr, R_{13} (O−H_b) ≈ R_{34} (H_b−H_c) ≈ 4 bohr, R_{14} (O−H_c) ≈ 2.3 bohr, and R_{23} (H_a−H_b) ≈ 2 bohr. After reaching this arrangement, atom H_b is quickly captured by the OH_c^+ ion previously formed in step 1. A schematic view of this characteristic configuration is shown in Figure 7. The consistent feature of this critical configuration that we found in many of the $H_2O^+ + H$ trajectories is a very interesting situation in which two sets of O−H and H−H bond lengths match, as can be seen in Figure 7.

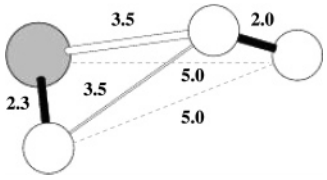

Figure 7. Characteristic geometry for formation of H_2O^+. The bond distances are in bohrs.

Discussion and Conclusions

The $O + H_3^+$ is a very interesting reaction system. The reactants are strongly attracted to one another and readily form an OH_3^+ complex (critical point I in Figures 1 and 2) at an energy of −100 kJ/mol. From this point, the system can go on to form $H_2O^+ + H$ with an overall energy of −158 kJ/mol.

However, this rarely happens even though the saddle point energy (critical point II) is only 30 kJ/mol above the energy of the OH_3^+ complex. Since the potential energy has dropped by 100 kJ/mol, the reactants have more than enough energy to overcome the 30 kJ/mol barrier. Over 90% of the time, the OH_3^+ complex falls apart to form OH^+ and H_2. These results are consistent with the narrow H_2O^+ exit channel shown on the potential energy contour plot and with the abrupt change in configuration required to enter this exit channel. An interesting aspect of the mechanism for the formation of H_2O^+ is that because of the large amount of available energy (~100 kJ/mol) the trajectories are not required to pass near the saddle point geometry. The bottleneck to reaction is obviously a dynamical bottleneck. We attempted to search for combinations of spatial and momentum coordinates that led to H_2O^+ formation, but this proved difficult with six spatial and six momentum coordinates. One characteristic we were able to uncover was that prior to the step 2 donation of the H′ atom to OH^+ the system often assumed a configuration in which $R_{O-H''} \approx R_{H''-H}$ and $R_{O-H'} \approx R_{H'-H}$. Listed below are some general conclusions for this study of the $O + H_3^+$ reaction system.

1. Increasing collisional energy decreases the cross sections in both reaction channels.

2. Adding a quanta of H_3^+ symmetric stretch has almost no effect on the cross sections in the $OH^+ + H_2$ channel; it produces a small increase in cross section for the $H_2O^+ + H$ channel.

3. Each diatomic product receives about 50% of the available energy in the OH^+ and H_2 channel; the OH^+ energy is predominately internal energy.

4. In the $H_2O^+ + H$ product channel, about 83% of the available energy is dumped into the H_2O^+ ion; less than 2% of the H_2O^+ product energy is translational energy.

5. O collisions with H_3^+ in the (100) excited vibrational state produces H_2O^+ that is more rotationally excited and with more energy in asymmetric stretch than H_2O^+ produced from ground vibrational H_3^+. O collisions with H_3^+ in the (100) excited vibrational state produces H_2 in the $OH^+ + H_2$ channel with twice the vibrational energy as H_2 produced from ground vibrational H_3^+.

6. H_2O^+ is produced from $O + H_3^+$ in a two-step process: H^+ transfer to O followed by H transfer to OH^+. The transfer of H^+ from H_3^+ to O produces OH^+ and H_2. These species become trapped in a potential well. While in this well, the atoms may reach a critical configuration that leads to transfer of a H atom to OH^+ to give H_2O^+.

It is our hope that this paper will encourage further theoretical and experimental studies of this very interesting reaction system.

Acknowledgment. The authors acknowledge and thank the Welch Foundation of Houston, Texas for support of this research.

References and Notes

(1) Fehsenfeld, F. C. *Astrophys. J.* **1976**, *209*, 638.
(2) Bettens, R. P. A.; Hansen; T. A.; Collins, M. A. *J. Chem. Phys.* **1999**, *111*, 6322.
(3) Frisch, M. J.; Trucks, G. W.; Schlegel, H. B.; Gill, P. M. W.; Johnson, B. G.; Robb, M. A.; Cheeseman, J. R.; Keith, T.; Petersson, G. A.; Montgomery, J. A.; Raghavachari, K.; Al-Laham, M. A.; Zakrzewski, V. G.; Ortiz, J. V.; Foresman, J. B.; Cioslowski, J.; Stefanov, B. B.; Nanayakkara, A.; Challacombe, M.; Peng, C. Y.; Ayala, P. Y.; Chen, W.; Wong, M. W.; Andres, J. L.; Replogle, E. S.; Gomperts, R.; Martin, R. L.; Fox, D. J.; Binkley, J. S.; Defrees, D. J.; Baker, J.; Stewart, J. P.; Head-Gordon, M.; Gonzalez, C.; Pople, J. A. *Gaussian 94*; Gaussian, Inc.: Pittsburgh, PA. 1995.
(4) Eaker, C. W.; Schwenke, D. W. *J. Chem. Phys*. **1995**, *103*, 6984.
(5) Eaker, C. W.; Schatz, G. C.; DeLeon, N.; Heller, E. J. *J. Chem. Phys.* **1984**, *81*, 5913.
(6) Simons, G.; Parr, R. G.; Finlan, J. M. *J. Chem. Phys*. **1973**, *59*, 3229.